Lawrence Berkeley National Laboratory

Title

Electronic structure of americium sesquioxide probed by resonant inelastic x-ray scattering

Permalink

https://escholarship.org/uc/item/1sc6581w

Journal

Physical Review B, 108(19)

ISSN

2469-9950

Authors

Butorin, SM

Shuh, DK

Publication Date

2023-11-01

DOI

10.1103/physrevb.108.195152

Copyright Information

Peer reviewed

Electronic structure of americium sesquioxide probed by resonant inelastic x-ray scattering

S. M. Butorin[1] and D. K. Shuh[2]

[1]*Condensed Matter Physics of Energy Materials,*
X-ray Photon Science, Department of Physics and Astronomy,
Uppsala University, P.O. Box 516, SE-751 20 Uppsala, Sweden
[2]*Chemical Sciences Division, Lawrence Berkeley National Laboratory,*
MS 70A1150, One Cyclotron Road, Berkeley, CA 94720, USA

The Am $5d$-$5f$ resonant inelastic x-ray scattering (RIXS) data of americium sesquioxide were measured at incident photon energies throughout the Am $O_{4,5}$ edges. The experiment was supported by calculations using several model approaches. While the experimental Am $O_{4,5}$ x-ray absorption spectrum of Am_2O_3 is compared with the spectra calculated in the framework of atomic multiplet and crystal-field multiplet theories and Anderson impurity model (AIM) for the Am(III) system, the recorded Am $5d$-$5f$ RIXS data are essentially reproduced by the crystal-field multiplet calculations. A combination of the experimental scattering geometry and theoretical analysis of the character of the electronic states probed during the RIXS process confirms that the ground state of Am_2O_3 is singlet Γ_1. An appearance of the low-intense charge-transfer satellite in the Am $5d$-$5f$ RIXS spectra at an energy loss of $\sim$5.5 eV, suggests weak Am $5f$-O $2p$ hybridization which is in agreement with AIM estimations of the $5f$ occupancy from spectroscopic data in Am_2O_3 as being 6.05 electrons.

I. INTRODUCTION

The importance of americium oxides in the nuclear cycle is well recognized. Besides the intention to have them as a part of fuels for the fourth generation (GEN IV) nuclear reactors, the use of these oxides for the power sources in the deep space missions is also being exploited [1–3]. However, the experimental studies of the electronic structure of americium oxides are scarce due to their substantial radioactivity.

X-ray spectroscopy is an important tool for this type of studies and allows for measurements on very small quantities of material in question. It can provide information about the chemical state of actinides in various systems, (non)stoichiometry, oxygen/metal (O/M) ratio, local symmetry of the environment and charge distribution, as well as other parameters important for nuclear fuel performance. One of the attractive techniques is resonant inelastic x-ray scattering (RIXS) which is very sensitive to changes in chemical state and in symmetry of the environment of the studied element, in particular by probing the elementary low-energy excitations ($5f$-$5f$ excitations in case of actinide systems). The availability of high resolution allows one to monitor the distribution of the electronic states in greater detail. In contrast to commonly used x-ray absorption spectroscopy (XAS), the RIXS resolution is not limited by the core-hole lifetime broadening and depends solely on the instrumental resolution. However, a number of pioneering valence-to-core RIXS studies at U $3d$ edges of uranium compounds [4–9] suffered from a limited resolution of utilized crystal-analyzers allowing one to resolve only the U $5f$-ligand $2p$ charge-transfer excitations which are mainly at higher energy losses than the $5f$-$5f$ excitations (only very recently, the high-resolution RIXS measurements at the U $3d$ edge became available [10]).

Soon after the experimental proof [11] that valence-to-core RIXS probes elementary electronic excitations (d-d excitations in case of MnO), going to shallow edges was a natural way to improve the resolution of the RIXS technique. The d-d RIXS measurements at the Cu $3p$ edge of the $Sr_2CuO_2Cl_2$ cuprate [12] followed by the measurements at the Ni $3p$ edge of NiO (Ref. [13, 14]) and $NdNiO_3$ (Ref. [13]) which indicated the ability of the technique to provide greater details on the d-d excitations. As to f-block systems, first RIXS measurements of f-f excitations at the $4d$ edges of lanthanides were performed for the Gd oxide [15], shortly followed by RIXS experiments for Ce-based heavy-fermion materials [16], while the first RIXS measurements at the $5d$ edges of actinides were carried out for UF_4 (Ref.[5]).

At actinide $5d$ thresholds, the main absorption edge is very broad due to so-called autoionization processes as it can be seen from XAS measurements (see e.g. Refs. [17–25]) and electron energy loss spectroscopy (EELS) [1, 26–31]. Such a broadening makes it difficult to determine the chemical shifts and obtain information about the ground state of the system from the XAS spectra. In this situation, the employment of the RIXS technique with its potentially unlimited resolution at the actinide $5d$ edges can be very helpful.

Although, initially pioneering $5d$-$5f$ RIXS studies at the actinide $O_{4,5}$ edges were carried out for oxides of uranium [23, 24, 32–35], neptunium [24, 34, 35] (see also the Supporting Information section of Ref. [36]), plutonium [24, 34] and curium [37], the RIXS technique at the actinide $5d$ edge was only rarely used because of safety restrictions for research on radioactive samples in the ultra-high vacuum environment at sources of synchrotron radiation.

Here we present first Am $5d$-$5f$ RIXS data of Am_2O_3 recorded at a number of incident photon energies at the Am $O_{4,5}$ edges. The data are analyzed with help of the

model calculations. The many-particle theoretical approaches turns out to be successful in reproducing the experimental spectra due to a significant localization of the $5f$ states in Am_2O_3.

II. EXPERIMENTAL

The Am oxide sample used for measurements was fabricated by technique used to prepare radionuclide counting plates at the Lawrence Berkeley National Laboratory (LBNL; see the "Preparation of counting sources" subsection in Ref. [38]). The counting plate was prepared from an aqueous solution of about 2.0 mM Am-243 (better than 99.6% Am-243 by mass) in 0.1 M HCl that was delivered by micropipette techniques to an area of $\sim$4 mm^2 area on a high purity Pt substrate (25.4 mm diameter). The aqueous droplets were allowed dry leaving a residue that was ring-shaped. This was followed by inductive heating to nearly 700 ^{o}C under atmosphere to oxidize the material and fixing the material to the Pt substrate to preclude loss when placed in the UHV spectrometer chamber during the measurement. This process is expected to yield the Am oxide sesquioxide with an approximate composition of Am_2O_3 (Ref.[37]). The counting plated was trimmed to 3 mm x 3 mm around the center and mounted on the sample holder with conductive tape as described below. The Am sample taken to the Advanced Light Source (ALS) was close to 1 μg of Am-243.

A specially designed sample holder, which is described in Refs. [24, 39], was used for the Am_2O_3 sample during the measurements. It is essentially a cylindrical can with slots for incoming and outgoing radiation. The sample is attached to the slab inside the can just behind the slot. Due to such a design, the sample holder served as a catch tray for material that might come loose during handling and the measurements, thus ensuring that no contamination will be left in the experimental chamber after the experiment.

Experiments in the energy range of the Am $O_{4,5}$ x-ray absorption edge ($5d \rightarrow 5f, 7p$ transitions) of Am_2O_3 were performed at beamline 7.0.1 of the ALS, LBNL employing a spherical grating monochromator [40]. The Am $5d$ XAS data were measured in the total electron yield (TEY) mode using drain current on the sample. The incidence angle of the incoming photons was close to 90° to the surface of the sample. The monochromator resolution was set to $\sim$50 meV at 115 eV during measurements at the Am $5d$ edge.

Am $5d$-$5f$ RIXS spectra of the sample at the Am $O_{4,5}$ x-ray absorption edge were recorded using a grazing-incidence grating spectrometer [41] with a two-dimensional detector. The 400 lines/mm grating of this spectrometer (based on the Rowland circle criterion) was employed to collect the RIXS data with the high energy resolution and the 300 lines/mm grating was used to measure the RIXS spectra in a larger energy range but with lower resolution. The incidence angle of the photon beam was 10° from the sample surface and the spectrometer was placed in the horizontal plane at an angle of 90°, with respect to the incidence beam. The total energy resolution of the RIXS spectra was estimated to be $\sim$70 meV for the 400 lines/mm grating and $\sim$160 meV for the 300 lines/mm grating, using the full-width at half maximum (FWHM) of the elastic peak. Measured RIXS spectra were normalized to the current in the ring.

III. COMPUTATIONAL DETAILS

The XAS spectra at the actinide $5d$ edges were calculated using the formalism described in Ref. [42] in order to account for the 'giant resonance', highly-inhomogeneous broadening of the spectral transitions (due to differences in core-hole lifetime of various core-excited states) and Fano effect. In our calculations, in addition to the interactions for the free ion, as used in Ref. [42], the crystal-field splittings in the $5f$ shell and the hybridization effects between actinide and oxygen states were taken into account using the Anderson impurity model (AIM) approach [43].

To simplify the calculations of the Am $5d$-$5f$ RIXS map around the Am(III) $O_{4,5}$ thresholds, the crystal-field multiplet theory approach was used because the Am $5f$-O $2p$ charge-transfer effects were not expected to be significant in americium sesquioxide (see e.g. Ref. [25]). The RIXS map was calculated using Kramers-Heisenberg equation

$$
\begin{aligned}
I_{qq'}(\omega,\omega') \; = \; & \sum_f \Big| \sum_m \frac{\langle f|D_{q'}|m\rangle\langle m|D_q|g\rangle}{E_g + \omega' - E_m - i\Gamma_m/2} \Big|^2 \\
& \times \delta(E_g + \omega' - E_f - \omega),
\end{aligned} \tag{1}
$$

where, $|g\rangle$, $|m\rangle$, and $|f\rangle$ are the ground, intermediate, and final states with energies E_g, E_m, and E_f, respectively, while ω' and ω represent energies of incident and scattered photons, respectively. D_q is the dipole operator, Γ stands for the intermediate state lifetime (Lorentzian FWHM) and q and q' are polarizations of the light with respect to the quantization axis. The experimental geometry for RIXS measurements was taken into account in the calculations as described in Ref. [44].

The required Slater integrals F^k, G^k and R^k, spin-orbit coupling constants ζ and matrix elements were obtained with the TT-MULTIPLETS package which combines Cowan's atomic multiplet program [45] (based on the Hartree-Fock method with relativistic corrections) and Butler's point-group program,[46] which were modified by Thole [47], as well as the charge-transfer program written by Thole and Ogasawara.
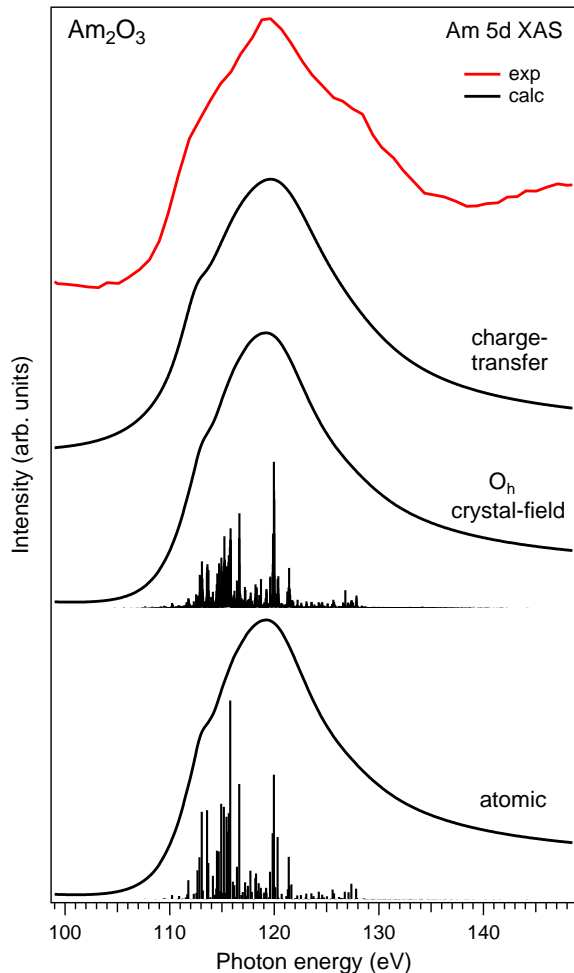
Figure 1. Expeimental and calculated XAS spectra at Am $O_{4,5}$ edges of Am_2O_3. The spectra are calculated using atomic and crystal-field multiplet theory for the Am^{3+} ion and Anderson impurity model, respectively.

Table I. The *ab-initio* Hartree-Fock values of Slater integrals and spin-orbit coupling constants for Am(III) ion. In XAS and RIXS calculations these values were reduced as described in the text. F, G and ζ are given in eV, R in $\sqrt{eV}$.

Am(III)	Value
$F^2(5f, 5f)$	10.086
$F^4(5f, 5f)$	6.577
$F^6(5f, 5f)$	4.823
$\zeta(5f)$	0.345
$F^2(5f, 5f)$	10.270
$F^4(5f, 5f)$	6.707
$F^6(5f, 5f)$	4.923
$\zeta(5f)$	0.359
$F^2(5d, 5f)$	11.434
$F^4(5d, 5f)$	7.377
$G^1(5d, 5f)$	13.599
$G^3(5d, 5f)$	8.412
$G^5(5d, 5f)$	6.005
$\zeta(5d)$	4.002
$R^1(5d\varepsilon g, 5f^2)$	1.208
$R^3(5d\varepsilon g, 5f^2)$	0.761
$R^5(5d\varepsilon g, 5f^2)$	0.540

Am_2O_3 compared with experimental one. First, the XAS spectrum was progressively calculated using atomic and crystal-field multiplet theory for the $(5d^{10}5f^6 \to 5d^95f^7)$ excitation of the Am(III) ion. Only the super-Coster-Kronig decay channel $(5d^{10}5f^6 \to 5d^95f^7 \to 5d^95f^5\varepsilon l)$ was taken into account in the calculations as a dominating process [42, 48].

It has been established (see e.g. [49–51]) that the Slater integrals describing the f-f interaction as well as the interaction of the f electrons with core holes in shallow levels such as $4d$ for lanthanides and $5d$ for actinides need to be scaled down from their *ab-initio* Hartree-Fock values for a description of the XAS spectra at those levels. In our calculations Slater integrals $F^k(5f, 5f)$, $F^k(5d, 5f)$, $G^k(5f, 5f)$ and $R^k(5d5f, 5d\varepsilon l)$ were reduced to 75%, 75%, 65% and 80%, respectively (see Table 1). The actual reduction values were also a result of the optimization of the agreement between calculated and measured Am $5d$-$5f$ RIXS spectra of Am_2O_3 (see below). Furthermore, the value of the spin-orbit coupling constant for the $5f$ shell was reduced in the calculations to 93% from the Hartree-Fock value for the same reason.

In the crystal-field multiplet calculations, Wybourne's crystal field parameters were set to B_0^4=-0.835 eV and B_0^6=0.100 eV based on the estimates for the case of Am(III) in ThO_2 [52]. In addition, the direct interatomic exchange and superexchange, treated as a magnetic field along the z-axis and acting on the spin S, were set to 0.001 eV to lift the degeneracy of the states.

Furthermore, the Am $O_{4,5}$ XAS spectrum of Am_2O_3 was calculated using the AIM approach (which also included the full multiplet structure) as shown in Fig. 1. The hybridization of Am $5f$ states with oxygen $2p$ states was taken into account in the AIM calculations for the Am(III) system. The same AIM parameter values were
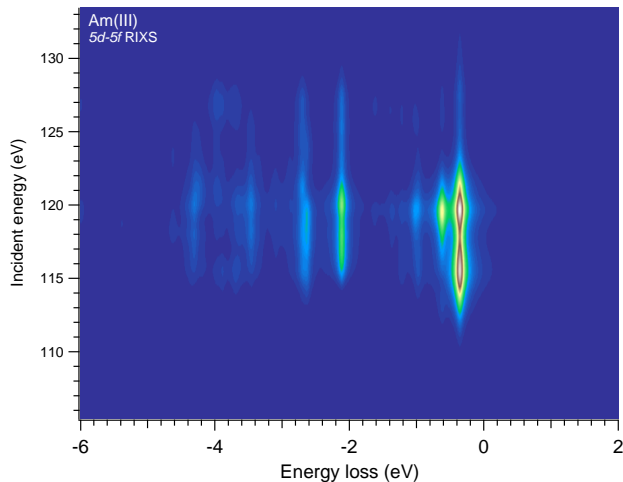
IV.   RESULTS AND DISCUSSION

The recorded Am $O_{4,5}$ XAS spectrum of Am_2O_3 is displayed in Fig. 1. For Am_2O_3, the autoinization processes can be characterized by three decay channels following the $5d^{10}5f^6 \to 5d^95f^7$ excitation. The $5d \to 5f$ absorption and $5d \to \varepsilon f$ ionization are competing routes coupled to each other by the $\langle 5d^95f^7|1/r|5d^95f^6\varepsilon f\rangle$ configuration interaction (CI). The decay of the excited $5d^95f^7$ states via $\langle 5d^95f^7|1/r|5d^95f^6\varepsilon f\rangle$ can be called the $5f \to \varepsilon f$ tunneling channel [42, 48]. The $5d^95f^7$ core excitations can also decay via $5d-5f5(s,p)$ Coster-Kronig and $5d-5f5f$ super-Coster-Kronig channels so that the excited states are coupled to the $5(s,p)^{-1}$ and $5f^{-1}$ ionization continua by the $\langle 5d^95f^7|1/r|5d^{10}5f^65(s,p)^{-1}\varepsilon l\rangle$ and $\langle 5d^95f^7|1/r|5d^{10}5f^5\varepsilon l\rangle$ CI processes, respectively. The broadening of the $5f$ edge which is highly inhomogeneous can be evaluated by calculating these CI matrix elements.

Fig. 1 shows the calculated Am $O_{4,5}$ XAS spectra of

Figure 2. Calculated Am $5d$-$5f$ RIXS map of Am_2O_3 using the crystal-field multiplet approach.

applied as in Ref. [25] where the Am $N_{4,5}$ XAS and $4f$ x-ray photoelectron spectra of Am_2O_3 were calculated. The ground state was described as a mixture of the $5f^6$ and $5f^7\upsilon^1$ configurations with Am $5f$-O $2p$ charge transfer energy Δ, $5f$-$5f$ Coulomb interaction U_{ff}, core-hole potential U_{fd} acting on the $5f$ electrons and Am $5f$-O $2p$ hybridization strength V were set to 6.5, 5.7, 6.0, and 0.7 eV, respectively.

An inspection of Fig. 1 reveals that the calculated XAS spectra are rather similar for all the three cases, i.e. taking into account the crystal-field interaction and Am $5f$-O $2p$ charge transfer does not lead to significant differences between calculated XAS spectra. This is because the ground state of Am_2O_3 is singlet Γ_1 (notations are for C_{4h} symmetry since the finite exchange field is applied along z-axis) and because the $O_{4,5}$ XAS spectrum is significantly broadened due to the autoionization processes. However, such a large core-hole lifetime broadening at the $5d$ edge does not affect the resolution of the $5d$-$5f$ RIXS spectra which mainly depends on the instrumental resolution in this case.

To make a comparison with experimental RIXS data, we calculated the Am $5d$-$5f$ RIXS map of Am_2O_3 for incident photon energies varying throughout the Am $O_{4,5}$ edges as shown in Fig. 2. For simplicity, the crystal-field multiplet approach was used since the contribution of the Am $5f$-O $2p$ charge transfer excitations to the RIXS spectra was expected to be small. The calculated RIXS intensities are displayed using the energy-loss scale in Fig. 2 and represent $5f$-$5f$ excitations. One can see that an elastic peak (at zero eV energy loss) is missing in the calculated spectra because the $5d$-$5f$ RIXS map in Fig. 2 was obtained for the scattering geometry used in our RIXS experiment. For the singlet Γ_1 ground state, the $\Gamma_1 \rightarrow 5d^9 5f^7 \rightarrow \Gamma_1$ transitions are forbidden for the scattering geometry employed. In this geometry, mainly Γ_3 and Γ_4 manifold states are probed as the final states of
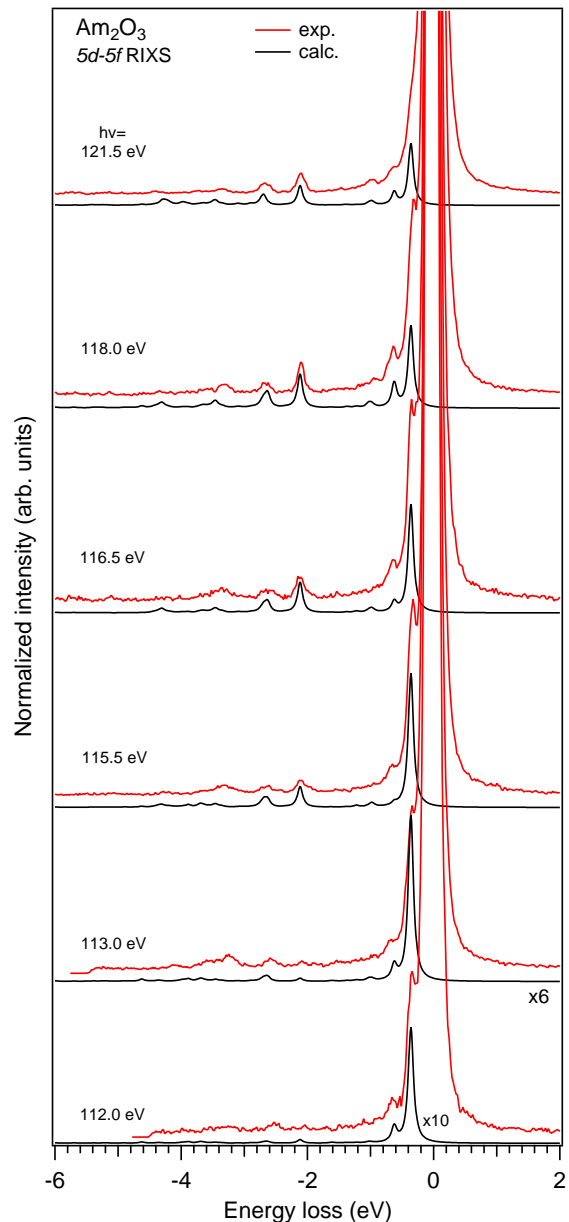

Figure 3. Experimental and calculated Am $5d$-$5f$ RIXS spectra of Am_2O_3 for several incident photon energies at Am $O_{4,5}$ edges.

the RIXS process. The first scattering structure which gains a non-zero intensity appears at an energy loss of 360 meV and is the most intense on the map.

The experimental Am $5d$-$5f$ RIXS spectra of Am_2O_3 recorded with the 400 lines/mm grating at several incident photon energies at the Am $O_{4,5}$ edges are compared with the calculated results in Fig. 3. All the experimental spectra have huge elastic peaks as a result of the reflectivity contribution in this energy range, nevertheless the first RIXS structure at $\sim$360 meV is still resolved in the recorded data. The calculated energies of the f-f
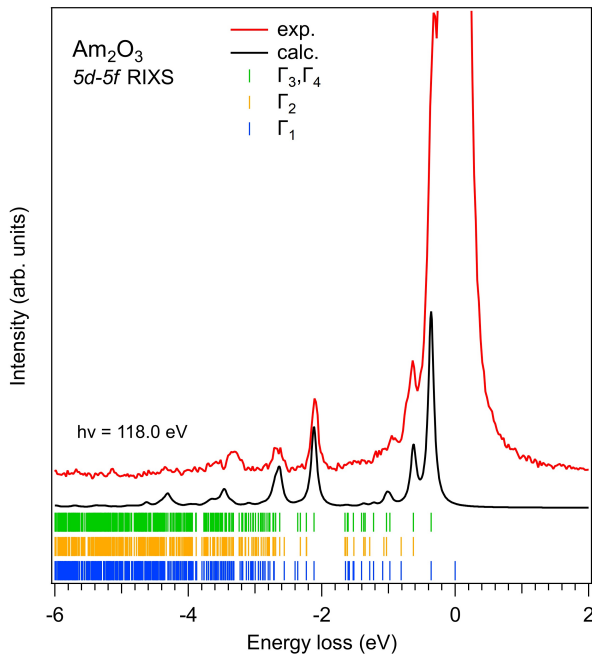
Figure 4. Measured and calculated Am $5d$-$5f$ RIXS spectra of Am_2O_3 at an incident photon energy of 118.0 eV together with calculated energy diagram for Γ_1, Γ_3, Γ_4 and Γ_2 states of the $5f^6$ ground state configuration.

(crystal-field) excitations and relative intensities of the calculated RIXS structures are in good correspondence with the measured ones (except for RIXS structures on the slope of the elastic peak). We avoided a subtraction of the elastic peak from experimental spectra because, for the correct procedure, elastic scattering needs to be measured from the surface with exactly the same (smooth) profile but without Am_2O_3 which is difficult to achieve.

An inspection of Fig. 3 shows the RIXS structures are not significantly resonating with varying incident photon energies as a result of the very short core-hole lifetime in the intermediate state of the RIXS process. Some dependence on the excitation energy can be seen for the structure at an energy loss of about 3.3 eV. As a whole, in contrast to the discussion on the dual character of $5f$ states in some actinide systems, a good agreement between calculated results and experimental data in our case indicates a significant localization of the $5f$ states in Am_2O_3.

The first RIXS structure at the energy loss of $\sim$360 meV corresponds to transitions to the Γ_4 and Γ_3 states which are split by 0.001 eV. This structure is characteristic for the Am(III) chemical state (see Fig. 4) and an existence of this structure in the RIXS spectra can be used to distinguish between Am(III) and Am(IV) compounds. Fig. 4 shows experimental and calculated Am $5d$-$5f$ RIXS spectra of Am_2O_3 at the incident photon energy of 118.0 eV together with the calculated energy diagram for the Γ_1, Γ_3, Γ_4 and Γ_2 states of the $5f^6$ ground state configuration. Such a comparison of spectra with
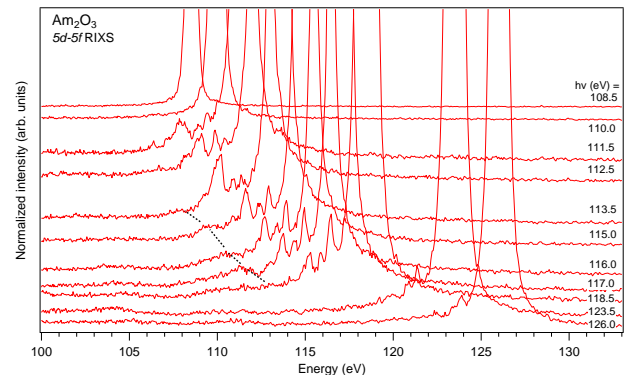

Figure 5. Am $5d$-$5f$ RIXS spectra of Am_2O_3 for several incident photon energies at Am $O_{4,5}$ edges measured with lower resolution but for a more extended energy range.

the energy diagram indicates the influence of the chosen scattering geometry on which states of the ground state configuration can be probed as a result of the RIXS process.

For RIXS spectra displayed in Fig. 3 which were recorded with the 400 lines/mm grating, the intensity is significantly cut-off for energy losses of around 5 eV and higher due to the use of the round detector (for example, a full cut-off is observed for a spectrum recorded at the incident energy of 112.0 eV). Therefore, the 300 lines/mm grating was used which provided the opportunity to measure the Am $5d$-$5f$ RIXS spectra for a more extended energy range but with lower resolution. Fig. 5 displays such spectra of Am_2O_3 for a number of the excitation energies on the incident photon energy scale. The excitation energies used can be identified by present huge elastic peaks. The $\sim$360-meV-energy-loss RIXS structure is not resolved but the resonating behavior of the $\sim$3.3-eV-energy-loss RIXS structure appears to be more distinct.

In RIXS spectra recorded at excitation energies between 113.5 and 117.0 eV, a new structure at $\sim$5.5 eV below the elastic peak can be identified which behavior upon changing excitation energy is indicated by a dashed line. This structure follows the increasing excitation energy (follows the elastic peak) and can be assigned to RIXS structures. Since the crystal-field multiplet calculations do not suggest the existence of the significant RIXS structures at the energy losses higher than 4.6 eV, the new structure can be attributed to the result of the Am $5f$-O $2p$ charge transfer (charge transfer satellite). For the description of the ground state as a mixture of the $5f^6$ and $5f^7\underline{\upsilon}^1$ configurations, the RIXS transitions to the anti-bonding combination of the Γ_1 character is also forbidden in the scattering geometry employed, while some transitions to the weakly bonded states of the $5f^7\underline{\upsilon}^1$ configuration are allowed (see also discussion in Ref. [44] related to RIXS spectra of CeO_2). These latter transitions are a result of an involvement of the O $2p$ states which are rather close to the valence band maximum.

The observed 5.5-eV energy loss of the charge-transfer satellite is consistent with the choice of the value of Am $5f$-O $2p$ charge-transfer energy Δ=6.5 eV as a parameter in our AIM calculations (see also Ref. [25]), because the Δ value is related to the center of the O $2p$ band.

and x-ray photoemission spectra of Am_2O_3 (Ref. [25]), estimating the $5f$ occupancy to be 6.05 electrons in the ground state.

V. CONCLUSIONS

The obtained Am $5d$-$5f$ RIXS data helps characterize the electronic structure of Am_2O_3. The observed agreement between recorded RIXS spectra and calculated results using the crystal-field multiplet approach indicates the significantly localized character of the Am $5f$ states in this oxide. The analysis of the RIXS structures by comparing the experimental and calculated data confirms that the ground state of Am_2O_3 is singlet Γ_1 of the $5f^6$ configuration. The experimental scattering geometry used, which leads to restrictions for specific RIXS transitions, made the analysis easier, despite the presence of the intense elastic peak due to high reflectivity contribution. The observation of the weak charge-transfer satellite in the Am $5d$-$5f$ RIXS spectra at the energy loss of $\sim$5.5 eV is consistent with Am $5f$-O $2p$ charge-transfer energy Δ=6.5 eV used in the AIM calculations of XAS

[1] T. Wiss, O. Dieste-Blanco, A. Tacu, A. Janssen, Z. Talip, J.-Y. Colle, P. Martin, and R. Konings, TEM study of alpha-damaged plutonium and americium dioxides, J. Mater. Res. **30**, 1544 (2015).

[2] J.-F. Vigier, D. Freis, P. Pöml, D. Prieur, P. Lajarge, S. Gardeur, A. Guiot, D. Bouëxière, and R. J. M. Konings, Optimization of Uranium-Doped Americium Oxide Synthesis for Space Application, Inorg. Chem. **57**, 4317 (2018).

[3] T. Wiss, D. Freis, J.-C. Griveau, K. Popa, J.-F. Vigier, J. Somers, E. D'Agata, R. Konings, O. Benes, J.-Y. Colle, and O. Dieste, Investigation on the use of Americium Oxide for Space Power Sources: Radiation Damage Studies, E3S Web Conf. **16**, 05004 (2017).

[4] S. M. Butorin, D. C. Mancini, J.-H. Guo, N. Wassdahl, J. Nordgren, M. Nakazawa, S. Tanaka, T. Uozumi, A. Kotani, Y. Ma, K. E. Myano, B. A. Karlin, and D. K. Shuh, Resonant X-Ray Fluorescence Spectroscopy of Correlated Systems: A Probe of Charge-Transfer Excitations, Phys. Rev. Lett. **77**, 574 (1996).

[5] S. M. Butorin, Resonant inelastic X-ray scattering as a probe of optical scale excitations in strongly electron-correlated systems: quasi-localized view, Journal of Electron Spectroscopy and Related Phenomena **110-111**, 213 (2000).

[6] D. A. Zatsepin, S. M. Butorin, D. C. Mancini, Y. Ma, K. E. Miyano, D. K. Shuh, and J. Nordgren, Strong anisotropy of resonant inelastic x-ray scattering from charge-transfer excitations in UO_3, Journal of Physics: Condensed Matter **14**, 2541 (2002).

[7] E. J. Nordgren, S. M. Butorin, L. C. Duda, J.-H. Guo, and J.-E. Rubensson, SOFT X-RAY FLUORESCENCE SPECTROSCOPY FOR MATERIALS SCIENCE AND CHEMICAL PHYSICS, in *Advanced Series in Physical Chemistry*, Vol. 12 (WORLD SCIENTIFIC, 2002) pp. 517–572.

[8] K. Kvashnina, Y. Kvashnin, and S. Butorin, Role of resonant inelastic X-ray scattering in high-resolution core-level spectroscopy of actinide materials, Journal of Electron Spectroscopy and Related Phenomena **194**, 27 (2014).

[9] K. O. Kvashnina, P. M. Kowalski, S. M. Butorin, G. Leinders, J. Pakarinen, R. Bès, H. Li, and M. Verwerft, Trends in the valence band electronic structures of mixed uranium oxides, Chem. Commun. **54**, 9757 (2018).

[10] A. Marino, M. Sundermann, D. S. Christovam, A. Amorese, C.-F. Chang, P. Dolmantas, A. H. Said, H. Gretarsson, B. Keimer, M. W. Haverkort, A. V. Andreev, L. Havela, P. Thalmeier, L. H. Tjeng, and A. Severing, Singlet magnetism in intermetallic UGa_2 unveiled by inelastic x-ray scattering, Phys. Rev. B **108**, 045142 (2023).

[11] S. M. Butorin, J.-H. Guo, M. Magnuson, P. Kuiper, and J. Nordgren, Low-energy d-d excitations in MnO studied by resonant x-ray fluorescence spectroscopy, Phys. Rev. B **54**, 4405 (1996).

[12] P. Kuiper, J.-H. Guo, C. Såthe, L.-C. Duda, J. Nordgren, J. J. M. Pothuizen, F. M. F. de Groot, and G. A. Sawatzky, Resonant X-Ray Raman Spectra of Cu dd Excitations in $Sr_2CuO_2Cl_2$, Phys. Rev. Lett. **80**, 5204 (1998).

[13] S. Butorin, C. Såthe, A. Agui, F. Saalem, J. Alonso, and J. Nordgren, Intra- versus inter-site electronic excitations in $NdNiO_3$ by resonant inelastic ultra-soft X-ray scatter-

ing at Ni 3p edge, Solid State Communications **135**, 716 (2005).

[14] S. G. Chiuzbăian, G. Ghiringhelli, C. Dallera, M. Grioni, P. Amann, X. Wang, L. Braicovich, and L. Patthey, Localized Electronic Excitations in NiO Studied with Resonant Inelastic X-Ray Scattering at the Ni *M* Threshold: Evidence of Spin Flip, Phys. Rev. Lett. **95**, 197402 (2005).

[15] A. Moewes, T. Eskildsen, D. L. Ederer, J. Wang, J. McGuire, and T. A. Callcott, Elastic and inelastic scattering of 4d inner-shell electrons in $(Y,Gd)_2O_3$ studied by synchrotron-radiation excitation, Phys. Rev. B **57**, R8059 (1998).

[16] S. Butorin, M. Magnuson, K. Ivanov, D. Shuh, T. Takahashi, S. Kunii, J.-H. Guo, and J. Nordgren, Resonant inelastic soft-X-ray scattering at the 4d edge of Ce-based heavy-fermion materials, Journal of Electron Spectroscopy and Related Phenomena **101-103**, 783 (1999).

[17] M. Aono, T.-C. Chiang, J. Weaver, and D. Eastman, Anomalous two-electron auger resonance in thorium near the $5d(O_5)$ photothreshold, Solid State Communications **39**, 1057 (1981).

[18] M. Iwan, E. E. Koch, and F.-J. Himpsel, Resonant 5f valence-band satellite at the 5d threshold in uranium metal, Phys. Rev. B **24**, 613 (1981).

[19] A. Fujimori and J. H. Weaver, Decay channels of the *5d→5f* excitation in thorium, Phys. Rev. B **31**, 6411 (1985).

[20] G. Kalkowski, G. Kaindl, W. D. Brewer, and W. Krone, Near-edge x-ray-absorption fine structure in uranium compounds, Phys. Rev. B **35**, 2667 (1987).

[21] L. E. Cox, W. P. Ellis, R. D. Cowan, J. W. Allen, S. J. Oh, I. Lindau, B. B. Pate, and A. J. Arko, Valence-band photoemission in UO_2 (111) near the *5d* resonant photon energy, Phys. Rev. B **35**, 5761 (1987).

[22] J. G. Tobin, B. W. Chung, R. K. Schulze, J. Terry, J. D. Farr, D. K. Shuh, K. Heinzelman, E. Rotenberg, G. D. Waddill, and G. Van Der Laan, Resonant photoemission in *f*-electron systems: Pu and Gd, Phys. Rev. B **68**, 155109 (2003).

[23] E. Nordgren, S. Butorin, L.-C. Duda, and J.-H. Guo, SOFT X-RAY EMISSION AND RESONANT INELASTIC X-RAY SCATTERING SPECTROSCOPY, in *Handbook of Applied Solid State Spectroscopy*, edited by D. R. Vij (Springer US, Boston, MA, 2006) pp. 595–659.

[24] S. M. Butorin, Resonant Inelastic Soft X-Ray Scattering Spectroscopy of Light-Actinide Materials, in *Actinide Nanoparticle Research*, edited by S. N. Kalmykov and M. A. Denecke (Springer Berlin Heidelberg, Berlin, Heidelberg, 2011) pp. 63–103.

[25] S. M. Butorin and D. K. Shuh, Chemical bonding in americium oxides probed by X-ray spectroscopy, Sci Rep **13**, 11607 (2023).

[26] M. Cukier, P. Dhez, B. Gauthé, P. Jaeglé, C. Wehenkel, and F. Combet Farnoux, Photoabsorption of Th and U by direct measurement and by fast electron energy loss spectra near the 5d thresholds, J. Phyique Lett. **39**, 315 (1978).

[27] H. R. Moser, B. Delley, W. D. Schneider, and Y. Baer, Characterization of *f* electrons in light lanthanide and actinide metals by electron-energy-loss and x-ray photoelectron spectroscopy, Phys. Rev. B **29**, 2947 (1984).

[28] S. B. Rice, H. H. Bales, J. R. Roth, and A. L. White-

side, Empirical Identification of Uranium Oxides and Fluorides Using Electron Energy-loss Spectroscopy in the Transmission Electron Microscope, Microsc Microanal **5**, 437 (1999).

[29] K. T. Moore and G. Van Der Laan, Nature of the 5f states in actinide metals, Rev. Mod. Phys. **81**, 235 (2009).

[30] J. A. Bradley, S. Sen Gupta, G. T. Seidler, K. T. Moore, M. W. Haverkort, G. A. Sawatzky, S. D. Conradson, D. L. Clark, S. A. Kozimor, and K. S. Boland, Probing electronic correlations in actinide materials using multipolar transitions, Phys. Rev. B **81**, 193104 (2010).

[31] C. Degueldre and L. Veleva, Electron energy loss spectroscopy investigations through nano-ablated actinide dioxide samples, Progress in Nuclear Energy **72**, 96 (2014).

[32] S. M. Butorin, D. K. Shuh, K. Kvashnina, I. L. Soroka, K. Ollila, K. E. Roberts, J.-H. Guo, L. Werme, and J. Nordgren, Resonant Inelastic Soft X-ray Scattering Studies of U(VI) Reduction on Iron Surfaces, MRS Proc. **807**, 113 (2003).

[33] D. K. Shuh, S. M. Butorin, J.-H. Guo, and J. Nordgren, Soft X-ray Synchrotron Radiation Investigations of Actinide Materials Systems Utilizing X-ray Emission Spectroscopy and Resonant Inelastic X-ray Scattering, MRS Proc. **802**, DD3.10 (2003).

[34] L. Werme, S. Butorin, and P. M. Oppeneer, The Role of the Actinides in a Performance Assessment of a Nuclear Waste Repository. SKB's Supporting Actinide Research, MRS Proc. **1265**, 1265 (2010).

[35] S. M. Butorin, D. K. Shuh, K. O. Kvashnina, J. Guo, L. Werme, and J. Nordgren, Chemical Reduction of Actinides Probed by Resonant Inelastic X-ray Scattering, Anal. Chem. **85**, 11196 (2013).

[36] S. M. Butorin, A. Modin, J. R. Vegelius, M.-T. Suzuki, P. M. Oppeneer, D. A. Andersson, and D. K. Shuh, Local Symmetry Effects in Actinide 4f X-ray Absorption in Oxides, Anal. Chem. **88**, 4169 (2016).

[37] K. O. Kvashnina, S. M. Butorin, D. K. Shuh, J.-H. Guo, L. Werme, and J. Nordgren, Resonant inelastic x-ray scattering of curium oxide, Phys. Rev. B **75**, 115107 (2007).

[38] K. J. Moody, D. A. Shaughnessy, K. Casteleyn, H. Ottmar, K. Lützenkirchen, M. Wallenius, and T. Wiss, Analytical Chemistry of Plutonium, in *The Chemistry of the Actinide and Transactinide Elements*, edited by L. R. Morss, N. M. Edelstein, and J. Fuger (Springer Netherlands, Dordrecht, 2010) pp. 3889–4003.

[39] D. E. Smiles and D. K. Shuh, Soft X-ray Synchrotron Radiation Studies of Plutonium Materials, in *Plutonium Handbook, 2nd Edition*, Vol. 6, edited by D. L. Clark, D. A. Geeson, and J. Hanrahan, R. J. (American Nuclear Society, 2019) pp. 2991–3007.

[40] T. Warwick, P. Heimann, D. Mossessian, W. McKinney, and H. Padmore, Performance of a high resolution, high flux density SGM undulator beamline at the ALS (invited), Review of Scientific Instruments **66**, 2037 (1995).

[41] J. Nordgren, G. Bray, S. Cramm, R. Nyholm, J. Rubensson, and N. Wassdahl, Soft x-ray emission spectroscopy using monochromatized synchrotron radiation (invited), Review of Scientific Instruments **60**, 1690 (1989).

[42] H. Ogasawara and A. Kotani, Calculation of Magnetic Circular Dichroism of Rare-Earth Elements, J. Phys. Soc. Jpn. **64**, 1394 (1995).

[43] P. W. Anderson, Localized Magnetic States in Metals,

Phys. Rev. **124**, 41 (1961).

[44] M. Nakazawa, H. Ogasawara, and A. Kotani, Theory of Polarization Dependence in Resonant X-Ray Emission Spectroscopy of Ce Compounds, J. Phys. Soc. Jpn. **69**, 4071 (2000).

[45] R. D. Cowan, *The theory of atomic structure and spectra*, Los Alamos series in basic and applied sciences No. 3 (University of California Press, Berkeley, 1981).

[46] P. H. Butler, *Point Group Symmetry Applications* (Springer US, Boston, MA, 1981).

[47] B. Thole, G. Van Der Laan, and P. Butler, Spin-mixed ground state of Fe phthalocyanine and the temperature-dependent branching ratio in X-ray absorption spectroscopy, Chemical Physics Letters **149**, 295 (1988).

[48] H. Ogasawara and A. Kotani, Calculation of rare-earth $4d$ giant-absorption spectra with multiplet effects and

decay processes, J Synchrotron Rad **8**, 220 (2001).

[49] J. Sugar, Potential-Barrier Effects in Photoabsorption. II. Interpretation of Photoabsorption Resonances in Lanthanide Metals at the 4d -Electron Threshold, Phys. Rev. B **5**, 1785 (1972).

[50] D. W. Lynch and R. D. Cowan, Effect of hybridization on $4d{\to}4f$ spectra in light lanthanides, Phys. Rev. B **36**, 9228 (1987).

[51] H. Ogasawara, A. Kotani, and B. T. Thole, Calculation of magnetic x-ray dichroism in $4d$ and $5d$ absorption spectra of actinides, Phys. Rev. B **44**, 2169 (1991).

[52] S. Hubert, P. Thouvenot, and N. Edelstein, Spectroscopic studies and crystal-field analyses of Am^{3+} and Eu^{3+} in the cubic-symmetry site of ThO_2, Phys. Rev. B **48**, 5751 (1993).